Journal of Solid State Chemistry **166,** 81–90 (2002)
doi:10.1006/jssc.2002.9563, available online at http://www.idealibrary.com on IDEAL®

Structural Study of $Li_{1+x-y}Nb_{1-x-3y}Ti_{x+4y}O_3$ Solid Solutions

L. Farber,* I. Levin,† A. Borisevich,* I. E. Grey,‡ R. S. Roth,† and P. K. Davies*,[1]

*Department of Materials Science and Engineering, University of Pennsylvania, Philadelphia, Pennsylvania 19104-6272; †Ceramics Division, NIST, Gaithersburg, Maryland 20899; and ‡CSIRO, Division of Minerals, Clayton, Australia

Received November 20, 2001; in revised form February 19, 2002; accepted February 22, 2002

The structures of $Li_{1+x-y}Nb_{1-x-3y}Ti_{x+4y}O_3$ solid solutions within the so-called *M*-phase field in the Li_2O–Nb_2O_5–TiO_2 system were investigated using high-resolution transmission electron, microscope (HRTEM) and single-crystal X-ray diffraction. The results demonstrated that the phase field is not a solid solution but rather a homologous series of commensurate intergrowth structures with $LiNbO_3$-type (LN) slabs separated by single $[Ti_2O_3]^{2+}$ corundum-type layers. The thickness of the LN slab decreases with increasing Ti-content from ~ 55 to 3 atomic layers in the metastable H-$Li_2Ti_3O_7$ end-member. The LN slabs accommodate a wide range of Ti^{4+}/Nb^{5+} substitution, and for a given homolog the distribution of Ti and Nb is not uniform across the slab. A single-crystal X-ray diffraction study of a structure composed of nine-layer LN slabs revealed preferential segregation of Ti to the slab surfaces which apparently provides partial compensation for the charge on the adjacent $[Ti_2O_3]^{2+}$ corundum layers. The extra cations in phases with $x > 0$ are accommodated through the formation of Li-rich Li_2MO_3-type layers in the middle of the LN slabs. The fraction of layers with extra cations increases with increasing Ti-content in the structure. © 2002 Elsevier Science (USA)

Key Words: **niobates; titanates; intergrowth structures; high resolution TEM; homologous series; lithium miobate.**

INTRODUCTION

The solid solution $Li_{1+x-y}Nb_{1-x-3y}Ti_{x+4y}O_3$, also referred to as the "*M*-phase," occurs over an extended phase field approximately in the center of the Li_2O–Nb_2O_5–TiO_2 ternary system (Fig. 1, cited by (1)). Recent studies have demonstrated that these solid solutions exhibit chemically tunable dielectric properties of interest for use in wireless communication systems ($\varepsilon = 55$–80, τ_f tunable to zero, $Q \times f$ up to 9000@6 GHz). Moreover, the relatively low sintering temperatures of these ceramics ($< 1100°C$) render them attractive candidates for low-temperature co-fired ceramic technology (LTCC) (2).

[1]To whom correspondence should be addressed. Fax: 215-573-2128. E-mail: davies@lrsm.upenn.edu.

Despite the technological potential of the *M*-phase solid solutions, their crystal chemistry has remained unclear. The initial studies of the *M*-phases showed that their powder X-ray patterns bear a strong resemblance to that of $LiNbO_3$ (LN) with the exception of several peak splittings and additional satellite reflections. Two different models have been proposed to describe the crystal structure of the *M*-phases. In one model, proposed by Smith and West for the Li_2O-rich end of the *M*-phase field (along the $LiNbO_3$–Li_2TiO_3 join), the solid solutions were described as having incommensurate structures comprised of random intergrowths of LN- and rocksalt-type Li_2TiO_3 slabs (3, 4). According to another model, (5) proposed by Roth and Davis for the structures along the $LiNbO_3$–$Li_4Ti_5O_{12}$ join, the *M*-phase field is comprised of a homologous series of commensurate structures based on ordered intergrowths of LN and a spinel-type end-member. Both models imply stacking faults in the oxygen packing at the interfaces between LN-type (hcp packing) and either rock-salt (ccp) or spinel (ccp) type slabs; however, no evidence was presented to support existence of such stacking defects in the oxygen subcell. Roth *et al.* noted the possible similarity of the *M*-phase structures to that of a metastable hexagonal (H) polymorph of $Li_2Ti_3O_7$ (6), later shown to contain 4-layer thick LN-type slabs separated by single layers of an unresolved nature (7). Minor additions of Nb_2O_5 were found to be effective in stabilizing H-$Li_2Ti_3O_7$ (8) and the structure of Nb_2O_5-doped H-$Li_2Ti_3O_7$ was solved recently by Rietveld analysis supplemented by high-resolution transmission electron microscope (HRTEM) data (9). The refinement demonstrated that the structure consists of LN slabs, five atomic layers thick, separated by a corundum-type $[Ti_2O_3]^{2+}$ layer. In this structure, the hcp stacking of oxygen is preserved across the interface between the LN and corundum-type slabs, which is in contrast to both models previously proposed for the *M*-phase

In the present work, we applied electron diffraction and structural imaging in a HRTEM combined with single-crystal X-ray diffraction to clarify the crystal structure of the $Li_{1+x-y}Nb_{1-x-3y}Ti_{x+4y}O_3$ solid solutions.

0022-4596/02 $35.00

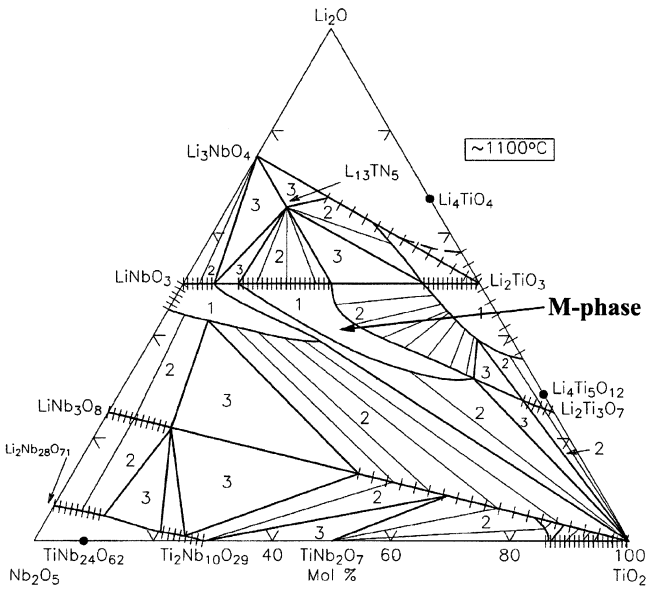

FIG. 1. Li_2O–TiO_2–Nb_2O_5 phase diagram at 1100°C (from Ref. (1)). The *M*-phase field is indicated.

TABLE 1
Average Block Lengths Computed from XRD for $Li_{1+x-y}Nb_{1-x-3y}Ti_{x+4y}O_3$ *M*-Phase Compositions

x	y	$\langle N \rangle$
0.1	0	49.76
0.15	0	35.87
0.2	0	26.90
0.1	0.025	22.44
0.15	0.025	16.76
0.05	0.05	18.61
0.1	0.05	15.66
0.05	0.075	16.77
0.1	0.075	11.95[a]
0.15	0.075	11.05[a]
0.05	0.1	15.22
0.1	0.1	9.98[a]
0.15	0.1	9.16[b]
0.1	0.125	9.03[a]
0.1	0.15	8.93[a]
0.1	0.175	8.85[c]

[a]Could be indexed as *M*-phases with N = closest integer.
[b]Could be indexed as a mixture of $N = 9$ and 10 *M*-phases.
[c]Could be indexed as a mixture of $N = 8$ and 9 *M*-phases

EXPERIMENTAL

The structural studies were conducted on polycrystalline ceramics prepared through a mixed oxide route, and flux-grown single crystals. The ceramic samples in the $Li_{1+x-y}Nb_{1-x-3y}Ti_{x+4y}O_3$ *M*-phase field were synthesized from dried Li_2CO_3 (Baker,[2] 99.0%), Nb_2O_5 (Cerac, 99.95%), and TiO_2 (Cerac, 99.9%) powders using several annealing and homogenization cycles (see details in (2)). The XRD patterns were recorded on a Rigaku DmaxB diffractometer using Cu$K\alpha$ radiation generated at 45 kV and 30 mA. The indexing scheme proposed by Roth and Davis (5) (see details in (2)) was used to determine the lattice parameters of the subcell and the average number of layers in the repeatable structural block $\langle N \rangle = \langle \#(\text{LN-type layers}) \rangle + \langle \#(\text{Ti-rich layers}) \rangle$. The compositions and their respective values of $\langle N \rangle$ are shown in Table 1.

Single crystals of the composition corresponding to a bulk stoichiometry of $Li_{9.5}Nb_{4.4}Ti_{7.1}O_{30}$ (with an $N = 10$-layer structure) were prepared by the flux method. A pre-reacted composition comprising 11.1 wt% Li_2O, 44.2 wt% Nb_2O_5, and 44.6 wt. TiO_2 was mixed with lithium molybdate (Li_2O:2.25 MoO_3) in the weight ratio 90:10, and the mixture was sealed in a platinum tube. The tube was heated at 1100°C for 119 h then removed from the furnace to cool. The excess flux was removed by washing with dilute HCl. The crystals were in the form of small colorless platelets, often with a hexagonal shape. A portion of the crystals was finely ground and a powder pattern obtained. This showed that the crystalline product was predominantly a single phase with 1–2% of rutile as the only impurity. The pattern could be completely indexed using hexagonal cell parameters which were refined to the values $a = 5.104(1)$ Å, $c = 23.190(1)$ Å. The compositions of the crystals were determined using wavelength-dispersive electron microprobe analysis, with $NbPO_5$ and TiO_2 as standards. Li could not be analyzed directly, but a good approximation to its analysis was obtained by subtracting the sum of the Nb and Ti contents from 100%. This value was then input into the data correction software to correct the Nb and Ti analyses for matrix effects due to the Li. Different crystals gave almost identical analyses, averaging (for seven crystals) 44.6 wt% Nb_2O_5, 43.8 wt% TiO_2.

Crystals from the flux run were initially examined using the precession method. This showed they had trigonal symmetry and that there were no systematic reflection extinctions. A small hexagonal platelet was selected for an intensity data collection, which was made using a Nonius Kappa diffractometer employing a CCD area detector. The data collection conditions are given in Table 2. The CCD intensity data set was processed to produce an absorption corrected file of F^2 and $\sigma(F^2)$ which was used with SHELXL (10) for the structure analysis.

The specimens for the TEM/HRTEM study were prepared by conventional cutting, grinding, and dimpling followed by ion thinning in a GATAN precision ion-polishing

[2]The use of brand or trade names does not imply endorsement of the product by NIST.

TABLE 2
Crystallographic Data for 10-Layer $Li_{9.5}Nb_{4.4}Ti_{7.1}O_{30}$

Crystal data	
Cell parameters (Å)	$a = 5.104(1)$, $c = 23.190(1)$
Z	1
Space group	P-3
Intensity measurements	Nonius Kappa/CCD
Temperature (K)	295
λ (Mo$K\alpha$)	0.71073
Crystal size (mm^3)	$0.07 \times 0.07 \times 0.025$
Collection mode	ϕ scan, 0–360°
	360 images at $\Delta\phi = 1°$
	150 s per image count time
Crystal-to-detector (mm)	45
2θ max	60°
Total no. of integrated reflections	5939 (= 99.6% data completeness)
No. unique reflections	1038
No. reflections, $F > 4\sigma(F)$	842
Absorption correction	Empirical, $\mu = 5.5\ mm^{-1}$
	$A_{min} = 0.77$, $A_{max} = 0.86$
R(merge) on F^2	0.066
Refinement	
No. parameters refined	82
G of F	1.09
$R1$, $F > 4\sigma(F)$	0.058
$R1$, all data	0.071

system. The electron-diffraction experiments were conducted in a Phillips EM 430 microscope operated at 200 kV. A JEOL3010-UHR microscope with a point-to-point resolution of 1.7 Å operated at 300 kV was used for structural imaging; the images were recorded with a GATAN charge-coupled device camera. Phase contrast simulations were performed using the Bloch waves formalism implemented in the EMS software package.

RESULTS

HRTEM

A representative [100] selected area electron-diffraction (SAED) pattern, collected from a single grain in the $Li_{9.5}Nb_{4.4}Ti_{7.1}O_{30}$ specimen, is shown in Fig. 2. The strongest (fundamental) reflections in this and other patterns collected from the specimens of different compositions were indexable according to an LN unit cell. The patterns feature sets of L extra reflections, Fig. 2, which divide the distance between the central and the 0006_{LN} reflection into $N = L + 1$ equal parts. Therefore, the diffraction patterns were attributed to a LN-based superstructure with a repeatable structural block (motif) containing $(L + 1) = N$ cation (or anion) layers along the c-axis of the hexagonal cell. For example, the $Li_{9.5}Nb_{4.4}Ti_{7.1}O_{30}$ specimen (Fig. 2) features a superstructure built of blocks that are 10-layers thick. To determine the applicability of HRTEM in understanding the structures of the $Li_{1+x-y}Nb_{1-x-3y}Ti_{x+4y}O_3$ solid solutions, phase contrast simulations were first performed for LN (11) and H-$Li_2Ti_3O_7$ (9) for various combinations of defocus and sample thickness (Fig. 3). The simulations for the [100] structural projection of both structures revealed a range of defocus-thickness conditions where a one-to-one correspondence exists between the Nb/Ti cation columns within the LN blocks and bright spots in the image. For the [210] projection of both structures, a similar correspondence was observed between the oxygen columns and bright spots in the images. Therefore, these two orientations provide an intuitive interpretation of the phase contrast in terms of the stacking sequence of the Nb/Ti and oxygen layers. In particular, the cubic stacking of Nb/Ti in the LN blocks should be revealed when the structure is imaged along [100] direction (Fig. 3a). The corundum-type layer in the simulated [100] image of H-$Li_2Ti_3O_7$ structure (Fig. 3c) exhibits different contrast and shifted position which disrupts the cubic closed-packed sequence of the Ti/Nb layers on going from one LN-type block to another. The images of both structures in the [210] orientation (Fig. 3b, d) reveal the continuous hexagonal stacking of oxygen layers.

Experimental HRTEM images of M-phase samples with different periodicities are presented in Fig. 4. The images collected in the [100] orientation (Figs. 4a–c) show that all

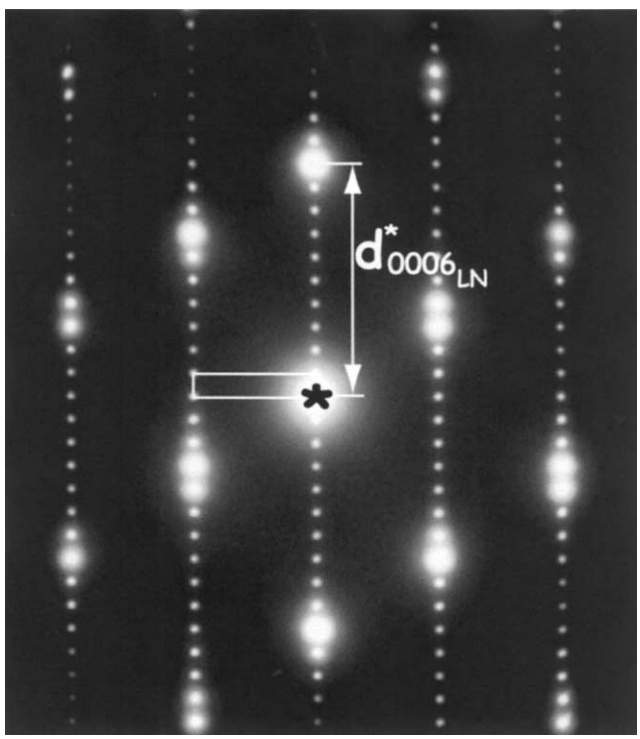

FIG. 2. Typical [100] electron diffraction pattern for M-phase samples collected from $N = 10$, single-crystal sample of $Li_{9.5}Nb_{4.4}Ti_{7.1}O_{30}$. The strongest reflections can be indexed according to the $LiNbO_3$ unit cell. The distance between the central and the 0006_{LN} reflections is subdivided into the $N = L + 1$ equal parts.

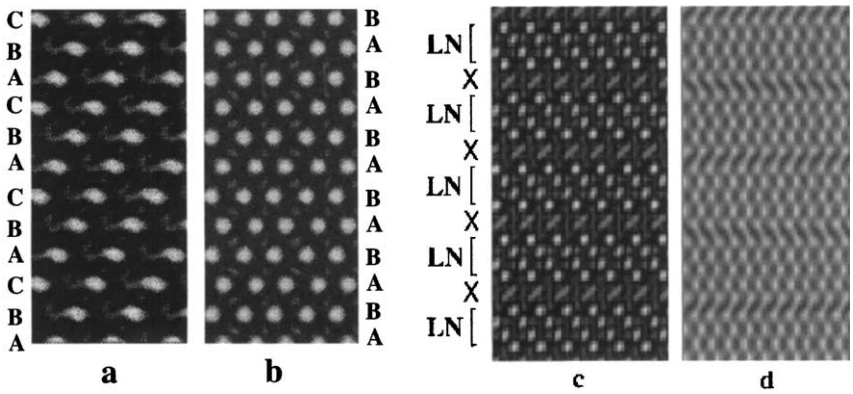

FIG. 3. Simulated HRTEM images for LN: (a) [100], defocus $\Delta f = -48$ nm, thickness $t = 25$ nm; (b) [210], $\Delta f = -32$, $t = 30$ nm and H-$Li_2Ti_3O_7$; (c) [100] defocus $\Delta f = -48$ nm, $t = 25$ and nm; and (d) [210] $\Delta f = -48$ nm, $t = 10$ nm. The Scherzer defocus for the JEOL-3010UHR microscope is about -36 nm.

of the structures are composed of blocks having cubic stacking of L cation layers separated by a single layer with different contrast and a shifted position. The resultant number of layers ($N = L + 1$) in the motif was in agreement with that observed in the corresponding SAED pattern. The phase-contrast images in the [100] orientation are very similar to those reported for the [100] orientation of H-$Li_2Ti_3O_7$ (9) and predicted by the phase-contrast simulations (Fig. 3c). The [210] images of all specimens, regardless of composition, revealed continuous hexagonal close-packing of oxygen (Fig. 4d) with no evidence for stacking faults. A close similarity between the phase contrast observed for

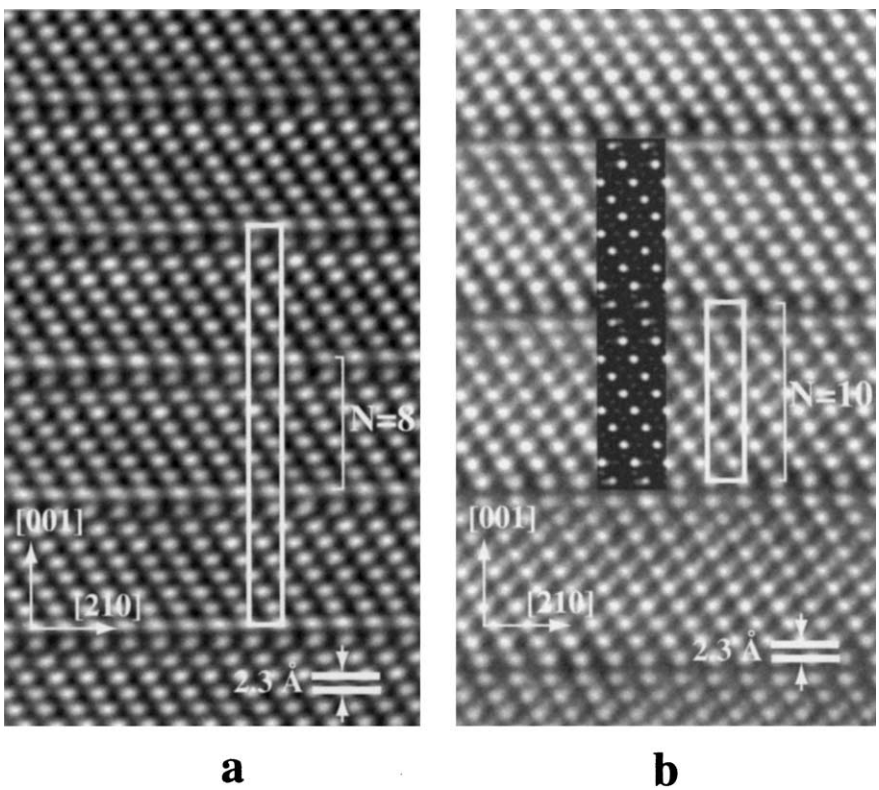

FIG. 4. (a–c) [100] HRTEM images of M-phases with $N = 8$ (a), $= 10$ (b) and $= 28$ (c), which reveal the packing of the Ti/Nb layers. The inset in (b) shows a phase-contrast image calculated using structural parameters obtained from the X-ray single-crystal refinement of the $N = 10$ structure. (d) A [110] HRTEM image of the $N = 28$ structure with a composition located on the $LiNbO_3$–Li_2TiO_3 join; the image reveals a continuous hexagonal close-packed sequence of the oxygen ions. Similar images were obtained for other M-phase compounds in this orientation. (e), (f) Electron diffraction patterns corresponding to the images given in (c), (d) with the strongest reflections indexed according to the LN unit cell.

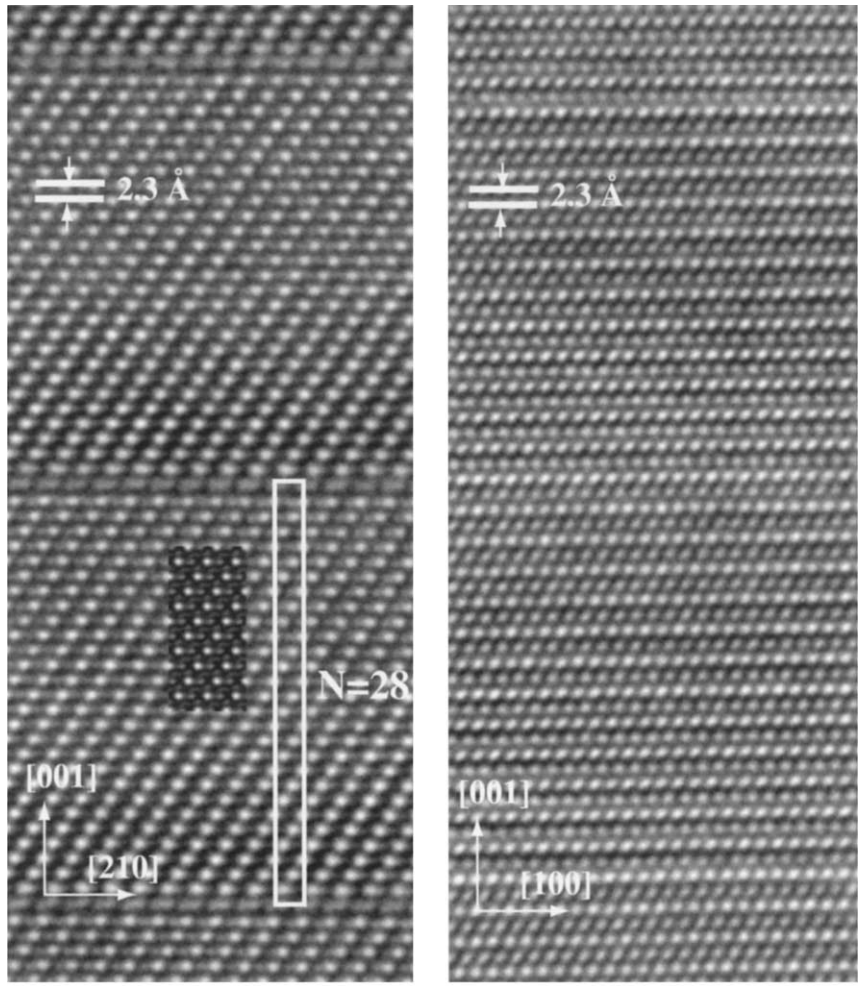

c d

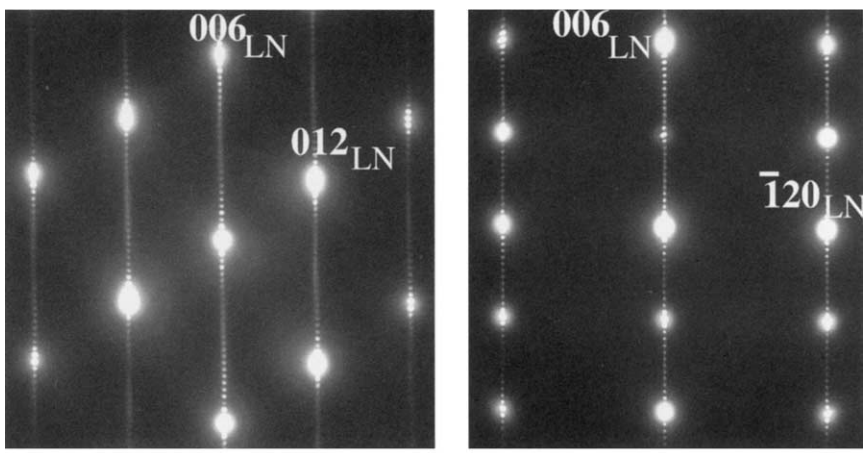

e f

FIG. 4—*Continued*

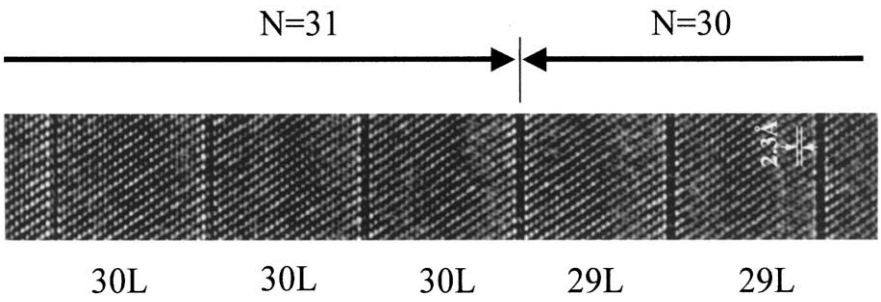

FIG. 5. Example of coherent intergrowth between different long period structures, in this case, $N = 31$ and 30.

the M-phases in both orientations and that of the H-$Li_2Ti_3O_7$ phase, suggest that the M-phases are also composed of LN-type slabs separated by corundum-type layers. This model for the M-phase was further confirmed by the single-crystal X-ray diffraction study of the $N = 10$ structure which is described below.

The results obtained for the number of cation layers (N) in a motif from the TEM studies were compared to the average values $\langle N \rangle$ calculated from the XRD data (Table 1). Generally, the compositions with small (10 or less) integer values of $\langle N \rangle$ in the XRD spectra appeared to be single phase with the same and unique value of N when investigated by TEM. Those with small non-integer $\langle N \rangle$ were found to contain two structures with the closest higher and lower integer values of N; for example a sample with $\langle N \rangle = 9.5$ is a mixture of $N = 9$ and 10. Samples with larger values of $\langle N \rangle$ were often comprised of more than two structures; for example, $\langle N \rangle = 26.9$ contained commensurate structures with N ranging from 25 to 31. The mixture of the structures was often realized in a form of coherent intergrowths, which was confirmed by tilting experiments and by HRTEM imaging; an example is shown in Fig. 5. Typically, the regions representing a particular structure (i.e., a single N value) were large enough to produce sharp superlattice reflections in the corresponding electron-diffraction patterns (Figs. 4e and f).

Single-Crystal X-Ray Refinement of $Li_{9.5}Nb_{4.4}Ti_{7.1}O_{30}$ ($N = 10$)

To validate the models presented above and understand the details of the atomic arrangements in the M-phases, structure refinements were conducted on a flux-grown crystal, $Li_{9.5}Nb_{4.4}Ti_{7.1}O_{30}$, with $N = 10$. A starting model for the Ti/Nb and O atom positions was developed based on the structure determination of H-$Li_2Ti_3O_7$ (9) with an hcp oxygen lattice and a 9-layer LN-type cation repeat separated by a $Ti_2O_3^{2+}$ corundum-type layer. Using the centrosymmetric $P\bar{3}$ space group (see discussion), a satisfactory refinement of the Ti/Nb and O positions was obtained. The

TABLE 3
Refined Structural Parameters for 10-Layer $Li_{9.5}Nb_{4.4}Ti_{7.1}O_{30}$

	Site	s.o.f.	x	y	Z	U_{eq}(Å^2)
M(1)	2d	0.333 Ti	$\frac{1}{3}$	$\frac{2}{3}$	− 0.01453(7)	0.007(1)
M(2)	2d	0.217(5) Ti + 0.116 Nb	$\frac{1}{3}$	$\frac{2}{3}$	0.11465(5)	0.005(1)
M(3)	2e	0.151(5) Ti + 0.182 Nb	0	0	0.20948(5)	0.010(1)
M(4)	2d	0.161(5) Ti + 0.172 Nb	$\frac{2}{3}$	$\frac{1}{3}$	0.30753(5)	0.010(1)
M(5)	2d	0.179(6) Ti + 0.154 Nb	$\frac{1}{3}$	$\frac{2}{3}$	0.40455(6)	0.014(1)
M(6)	1b	0.085(4) Ti + 0.082 Nb	0	0	$\frac{1}{2}$	0.010(1)
Li(1)	2e	0.327(3) Li + 0.006 Ti	0	0	0.0860(6)	0.01
Li(2)	2d	0.311(5) Li + 0.022 Ti	$\frac{2}{3}$	$\frac{1}{3}$	0.1817(5)	0.01
Li(3)	2d	0.310(4) Li + 0.023 Ti	$\frac{1}{3}$	$\frac{2}{3}$	0.2841(5)	0.01
Li(4)	2e	0.333 Li	0	0	0.3768(9)	0.01
Li(5)[a]	2d	0.333 Li	$\frac{2}{3}$	$\frac{1}{3}$	0.482(1)	0.01
O(1)	6g		0.025(1)	0.383(1)	0.0492(2)	0.012(1)
O(2)	6g		0.289(1)	0.321(1)	0.1507(2)	0.009(1)
O(3)	6g		0.953(1)	0.294(1)	0.2502(2)	0.010(1)
O(4)	6g		0.621(1)	0.994(1)	0.3503(2)	0.009(1)
O(5)	6g		0.044(1)	0.331(1)	0.4500(2)	0.010(1)

[a]Li(5) is split between two sites with $z = 0.482$, s.o.f = 0.22(1), and $z = 0.427$, s.o.f. = 0.11.

positions of the Li atoms were obtained from difference Fourier maps. The refinement was continued with allowance for mixed occupancy of the metal atom sites by Nb and Ti and for partial occupancy of the Li sites by Ti/Nb. The final refinement incorporated anisotropic thermal parameters for the Ti/Nb and O atoms. The refinement details are given in Table 2. The refined atomic coordinates, equivalent isotropic thermal parameters, and site occupancies are given in Table 3.

A polyhedral representation of the structure of the 10-layer phase is shown projected along [110] in Fig. 6. The refinement confirms a close structural relationship to the 5-layer H-$Li_2Ti_3O_7$ phase, for which the actual composition is $Li_{4.6}Nb_{0.2}Ti_{6.1}O_{15}$ (9). In particular, it comprises an ordered intergrowth, parallel to (001), of corundum-type M_2O_3 layers with 9-layer wide LN-type blocks (compared to 4 layers of LN in $Li_{4.6}Nb_{0.2}Ti_{6.1}O_{15}$). The Ti atoms are fully ordered in the $M(1)O_6$ octahedra of the M_2O_3 layers and are also preferentially ordered in the $M(2)O_6$ octahedra in adjacent layers. The $M(1)O_6$ and $M(2)O_6$ octahedra share a common octahedral face as in corundum. The $M(3)$–M(6) sites in the LN blocks contain approximately equal amounts of Ti and Nb. Phase-contrast images simulated using the refined structural parameters were consistent with those observed experimentally for the ceramic specimen of the same nominal composition (Fig. 4b).

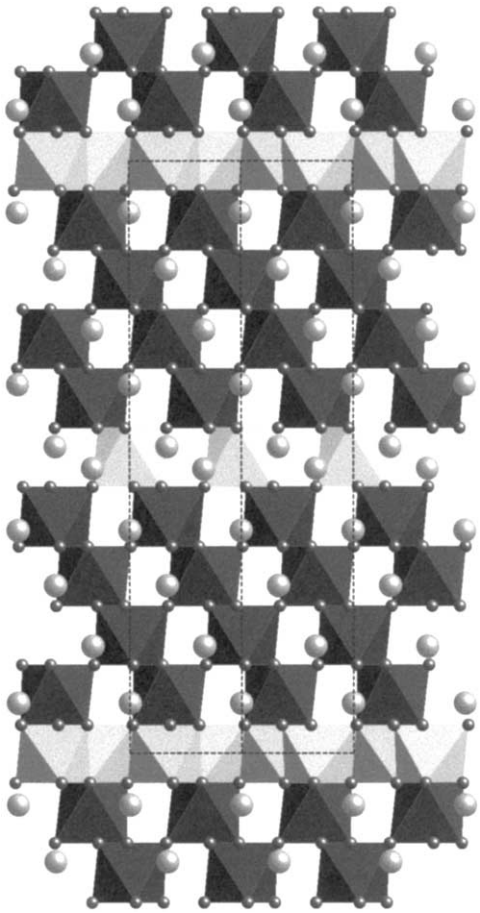

FIG. 6. Polyhedral representation of the 10-layer structure projected along [110]. The unit cell outline is shown with the *c*-axis vertical. The gray circles are Li atoms, the corundum-type M_2O_3 octahedral layers are gray, the LN-type octahedra are black, and the octahedra in the Li_2MO_3 layer are off-white.

The $M(2)$ atoms in the LN layers adjacent to the $M(1)_2O_3$ layer are displaced along [001] due to octahedral face-shared repulsions with the $M(1)$ atoms. The displacements are in opposite directions on either side of the M_2O_3 layer and they influence the metal atom displacements in subsequent LN layers. This results in ferroelectric LN blocks of opposite polarity on opposite sides of the M_2O_3 layers. Connectivity of these oppositely poled regions is made via a layer with a structure closely related to paraelectric LN(12). This region is shown by the off-white shading in Fig. 6. In the paraelectric region, the $M(6)$ atoms are located midway between the oxygen layers, and the Li(5) atoms are located close to the plane of the oxygen atoms. As in paraelectric LN, the Li(5) atoms are disordered over two sites on either side of the plane of the oxygen atoms. The composition of the paraelectric layer is formally Li_2MO_3.

The layer sequence in the 10-layer structure is M_2O_3–4($LiMO_3$)–Li_2MO_3–4($LiMO_3$), giving an ideal composition $Li_{10}M_{11}O_{30}$. However, the actual composition contains less than 10 Li atoms because of partial substitution of Li(2) and Li(3) by M in the two central layers of the ferroelectric LN blocks, see Table 3. This type of substitution was also found in the 5-layer $Li_{4.6}Nb_{0.2}Ti_{6.1}O_{15}$ (9) and it has been extensively studied in non-stoichiometric $Li_{1-5x}Nb_{1+x}O_3$ (13). In the latter compound, the substitution is accompanied by Li-site vacancies. We were unable to determine if Li-site vacancies played a role in this study because of the complication of three different metal atoms.

The unit cell composition derived from the site occupation factor refinements, Table 3, is $Li_{9.69}Nb_{4.24}Ti_{7.07}O_{30}$. The sum of the cation charges is + 59.2. Small adjustments (< 1 e.s.d. of the s.o.f.'s) to the composition to achieve charge balance gives a unit-cell composition $Li_{9.5}Nb_{4.4}Ti_{7.1}O_{30}$. The oxide contents for this composition are 45.2 wt% Nb_2O_5 and 43.8 wt% TiO_2, which are in good agreement with the microprobe results of 44.6 wt% Nb_2O_5 and 43.8 wt% TiO_2.

Selected interatomic distances for $Li_{9.5}Nb_{4.4}Ti_{7.1}O_{30}$ are given in Table 4. The $M(1)O_6$ octahedra in the corundum-type layer, and the octahedra containing $M(2)$ to $M(5)$ in the ferroelectric LN layers all have three longer bonds (2.02–2.11 Å) and three shorter bonds (1.86–1.92 Å), as observed in corundum-type structures and in ferroelectric LN. The difference between the long and short bonds gets progressively smaller in the sequence $M(2)$–$M(5)$ as the layers approach the paraelectric LN region. The $M(6)O_6$ octahedron is centered on a special position in the paraelectric LN

TABLE 4
Selected Interatomic Distances for 10-Layer $Li_{9.5}Nb_{4.4}Ti_{7.1}O_{30}$

	Distance (Å)		Distance (Å)
M(1)–O(1) ×3	1.892(4)	Li(1)–O(1) ×3	2.082(7)
–O(1) ×3	2.114(4)	–O(2) ×3	2.167(10)
–M(1) edge	3.023(1)	–M(2) edge	3.021(3)
–M(2) face	2.996(2)	–M(3) face	2.863(14)
M(2)–O(2) ×3	1.859(4)	Li(2)–O(2) ×3	2.029(6)
–O(1) ×3	2.147(4)	–O(3) ×3	2.233(9)
		–M(3) edge	3.016(3)
M(3)–O(3) ×3	1.888(4)	–M(4) face	2.918(12)
–O(2) ×3	2.075(4)		
M(4)–O(4) ×3	1.907(4)	Li(3)–O(3) ×3	2.075(6)
–O(3) ×3	2.058(4)	–O(4) ×3	2.202(9)
		–M(4) edge	2.996(2)
M(5)–O(5) ×3	1.922(4)	–M(5) face	2.793(11)
–O(4) ×3	2.019(4)		
M(6)–O(5) ×6	1.968(4)	Li(4)–O(4) ×3	2.014(8)
–Li(4) face	2.857(21)	–O(5) ×3	2.326(16)
–Li(5) edge	2.981(4)		
M(5)–Li(4) edge	3.016(4)	Li(5)–O(5) ×3	2.056(11)
–Li(5) face	2.668(29)	–O(5) ×3	2.278(21)

layer and has six equal M–O distances of 1.968(4) Å. The LiO_6 octahedra also have three shorter and three longer bonds. The two Li–O distances are similar to those in ferroelectric LN (12).

In $Li_{9.5}Nb_{4.4}Ti_{7.1}O_{30}$, the ~10 Li atoms are compressed into 9 layers, rather than 10 layers as in LN. As a consequence, the Li–Nb distances in the face-shared octahedra of the LN blocks are considerably shorter, 2.67–92 Å, than in LN (Li–Nb = 3.05 Å). The M(1)–M(2) distance of 2.996(2) Å across the shared octahedral face in the corundum-type region is the same as obtained for the 5-layer intergrowth (9).

DISCUSSION

The main goal of this investigation was to determine the appropriate structure model(s) for different compositions of the M-phase solid solutions in the Li_2O–Nb_2O_5–TiO_2 system. All of our results are consistent with a description of the M-phase field as a homologous series of commensurate structures. Both the single-crystal X-ray diffraction study and HRTEM confirmed the close similarity of the M-phase structures to that of H-$Li_2Ti_3O_7$. The basic elements of the M-phase structure are L-layer thick LN slabs separated by a single corundum-like $[M_2O_3]^{2+}$ layer, giving structural motif with $(L + 1) = N$ cation (or anion) layers along the c-axis. The LN-type slabs exhibit a cubic close-packed stacking sequence of the Nb/Ti layers. The location of the Ti cations in the extra layer does not correspond to the close-packed stacking, although it depends on the position of the two surrounding cation layers. The resulting layer sequence for the Nb(Ti) cations (for example for the $N = 5$ structure) can be described as …{abca[**a** + **b**]bcab[**b** + **c**]cabc [**c** + **a**]} abca [**a** + **b**]bca …, where the positions of Ti(Nb) cations within the intermediate layer are indicated using bold letters enclosed in square brackets. In this case, the c-axis periodicity for the cation sublattice (denoted by curved brackets) is $3N = 15$ layers. The oxygen stacking is hexagonal and continuous throughout the Ti-rich corundum layers. No evidence was found for stacking faults in the oxygen subcell in any of the compositions investigated (including $LiNbO_3$–Li_2TiO_3 join), thus, ruling out the previously suggested intergrowth models (3, 5). Since the hcp oxygen sublattice has a 2 layer repeat, the total lattice periodicity must always include an even number of atomic layers. Thus, the overall periodicity in the example above is 30 layers with $c = 30d_{001}$, where d_{001} is the average spacing between the atomic layers.

The symmetry and the c-lattice parameter of the M-phase structures depend on the number of layers L in the LN slab. The {001} LN slabs exhibit $p\bar{3}$ layer symmetry. The Bravais lattices for the structures with $L = 3k$ (k = any integer) and $L \neq 3k$ are primitive (P) and rhombohedral (R), respectively. Thus, for structures with $L = 3k$ odd and $L \neq 3k$ odd, the resultant space groups are $P\bar{3}$ ($c = Nd_{001}$) and $R\bar{3}$ ($c = 3Nd_{001}$), respectively. For L even (N odd), the additional doubling of the unit cell generates a c-glide plane with $P\bar{3}c1$ and $R\bar{3}c$ symmetry for $L = 3k$ even and $L \neq 3k$ even, respectively. These four space groups (Table 5), account for all possible structural arrangements in the M-phases (assuming ideal atomic positions). The observed diffraction patterns for the structures studied were in full agreement with the symmetries predicted.

Each composition within the phase field should be either single phase (for integer $\langle N \rangle$) or a two-phase mixture (for non-integer $\langle N \rangle$). The fact that more than two phases with different but close N's were typically observed in samples with low Ti content (large $\langle N \rangle$) suggests that equilibrium in these cases is very difficult to achieve because of small free-energy differences between the higher N structures.

At 1100–1150°C, the stable structures have LN slabs with L ranging from 7 to 55 (2, 5). However, additional structures

TABLE 5
Space Group of the M-Phases as a Function of the Number of Layers in $LiNbO_3$-Type Block L (k — Any Positive Integer)

L ($= N - 1$)		c lattice parameter	Space group
$= 3k$ (P symm. cell)	Even	$2N \times D_{001}$	$P\bar{3}c1$
	Odd	$N \times D_{001}$	$P\bar{3}$
$\neq 3k$ (R symm. cell)	Even	$6N \times D_{001}$	$R\bar{3}c$
	Odd	$3N \times D_{001}$	$R\bar{3}$

with $L = 4$, 5, and 6 can be obtained under different conditions (5), with their compositions lying close to the line between the 1100°C extreme ($L = 7$) and $Li_2Ti_3O_7$. Zou *et al.* (7) also reported the $L = 3$ polymorph of metastable H-$Li_2Ti_3O_7$. Apparently, the high levels of Ti in the LN slabs decrease the stability of the lower-N homologues, which become metastable for the Nb-free compounds.

One of the primary crystal chemical features of the M-phase structures is the accommodation of Ti in the $[Ti_2O_3]^{2+}$ corundum block. In all the samples investigated, the width of this block was restricted to a single layer, which is consistent with it carrying a charge. Therefore, changes in the chemical composition of the $Li_{1+x-y}Nb_{1-x-3y}Ti_{x+4y}O_3$ M-phases must be accommodated by alterations in both the length (L) and chemistry of the LN slabs. This is supported by the previous studies of the system using powder XRD (2, 5), which found a well-defined correlation between the mean length L of the LN slabs and the Ti content (or equivalently the (Li + Nb)/Ti ratio). The large number of homologues leads to very narrow compositional ranges of stability with respect to the (Li + Nb)/Ti ratio for any single member of series. For example, small deviations in the Ti content in a ceramic sample of $Li_{9.5}Nb_{4.4}Ti_{7.1}O_{30}$ ($N = 8$), resulted in 2-phase mixtures of $N = 8$ and 7 (Ti-rich) or N = 8 and 9 (Ti-deficient). In contrast, the periodicity of the structure is relatively insensitive to changes in the Li/Nb ratio and, for a given Ti content, variable degrees of excess cations within the LN slab can be accommodated without any change in N (see discussion below).

While the structural periodicity for a given phase translates directly into the proportion of $[Ti_2O_3]^{2+}$ layers, this is not the only compositional parameter that changes from one homologue to another. Both the shape of the phase field and the structure refinements for $N = 5$ (12) and $N = 10$ (this study), indicate that the relative concentration of Ti in the LN-type slabs varies among different phases. For example, in the stabilized end-member of the series, H-$Li_2Ti_3O_7$, almost all of the Nb is replaced by Ti. These differences are reflected by changes in the a lattice parameter, which were discussed in detail in a previous study (2). The single-crystal X-ray diffraction studies also confirm that Nb and Ti are not uniformly distributed throughout the LN slabs. In particular, Ti preferentially segregates toward the LN-block surfaces, so that the compositions of the outer cation layers in these blocks approach a stoichiometry $[LiTiO_3]^{1-}$; apparently, this segregation of Ti occurs to offset a local excess of positive charge of the adjacent $[Ti_2O_3]^{2+}$ corundum block. Thus, each structure uniquely accommodates Ti by a combination of a certain block length (L) and a specific distribution of Ti within the blocks. Speculations on the finer details of this distribution would require additional structural information.

Another important parameter affecting the cation distribution is the site stoichiometry. While $LiNbO_3$ and $[Ti_2O_3]^{2+}$ both have perfect M_2O_3 stoichiometry, the $Li_{1+x-y}Nb_{1-x-3y}Ti_{x+4y}O_3$ M-phase can accommodate a significant proportion of excess cations, with x varying from 0.05 to 0.2 in the compositions investigated. The neutron diffraction studies of $N = 5$ (12) and the X-ray study of $N = 10$ both indicate that the extra cations are accommodated through the insertion of Li into the middle of each LN block. This central region approaches a stoichiometry Li_2MO_3 and has a structure similar to that of paraelectric $LiNbO_3$. For the $N = 5$ composition ($x = 0.21$, $y = 0.252$), the additional lithium cations ($5x = 1$/block) are accommodated within the close-packed anion layer in the center of the block. If the additional Li ions are assigned equally to the adjacent LN layers and the minor niobia substitution is ignored (12), the structure has a $\{(Ti_2O_3)^{2+}(Li_{0.97}Ti_{1.03}O_3)^{0.9-}(Li_{1.35}Ti_{1.14}O_3)^{0.1-}(Li_{1.35}Ti_{1.14}O_3)^{0.1-}(Li_{0.97}Ti_{1.03}O_3)^{0.9-})\}$ layer sequence. In this case, the two central LN layers have $M_{2.5}O_3$ stoichiometry. In the $N = 10$ $Li_{9.5}Nb_{4.4}Ti_{7.1}O_{30}$ ($x = 0.1$, $y = 0.152$) structure (which was refined by X-rays and is subject to greater error for the occupancies and positions of Li and O), the additional Li ($10x = 1$/block) is again accommodated by central LN layers with LiM_2O_3 stoichiometry and the layer sequence is $\{M_2O_3$–4($LiMO_3$)–Li_2MO_3–4($LiMO_3$)$\}$. Homologues with both large and small values of N exhibit similar concentrations of excess cations (e.g., for $N = 26$, $x = 0.2$). However, the number of such cations (5.2/block for $N = 26$), that must be inserted into the LN slab, increases with increasing N. In such structures, several layers in the middle of the LN slab must contain additional Li cations. For a fixed x-value, the number of layers with a cation to anion ratio greater than 2:3 increases with increasing N; however, the fraction of layers with extra cations decreases. For example, the extra cations in $N = 26$ could be accommodated if 5 of the layers (20%) in the LN slab have Li_2MO_3-type stoichiometry. In the corresponding $N = 5$ structure, 50% of the LN layers contain excess Li. This may be an additional factor contributing to the reduced stability of the lower N phases.

The application of HRTEM played a key role in establishing that the M-phase field is comprised of a homologous series of commensurate structures. While compositions with low N (5–12) adjacent to the $LiNbO_3$–H-$Li_2Ti_3O_7$ join could generally be produced in the form of single-phase specimens and solved by X-ray refinement, those having high N usually produce a mixture of several phases. For this reason, it is unlikely that further studies of the high N phases using neutron or X-ray diffraction would yield reliable additional information on the details of the cation site occupancies.

Finally, the results of this study proved to be applicable to the Li_2O–Ta_2O_5–TiO_2 system where a similar, but narrower region of M-phase solid solutions has been identified. Our preliminary results indicate that the

$Li_{1+x-y}Ta_{1-x-3y}Ti_{x+4y}O_3$ solid solutions are isostructural with their Nb counterparts (14).

SUMMARY

The structures of $Li_{1+x-y}Nb_{1-x-3y}Ti_{x+4y}O_3$ M-phase "solid solutions" were studied by HRTEM and single-crystal X-ray diffraction. The M-phase field actually contains a homologous series of commensurate intergrowth structures comprised of $LiNbO_3$-type (LN) slabs of thickness L separated by single $[Ti_2O_3]^{2+}$ layers with a corundum-type structure. The number of layers in the LN slab decreases as the concentration of Ti is increased ranging from ~ 55 to 3 in the metastable H-$Li_2Ti_3O_7$ end-member. The LN slabs accommodate a wide range of Ti^{4+}/Nb^{5+} substitution. For a given homologue, the distribution of Ti and Nb is not uniform throughout the slab. By approaching a $[LiTiO_3]^{1-}$ stoichiometry, the layers at the edge of the LN slab tend to offset the positively charged adjacent $[Ti_2O_3]^{2+}$ corundum layers. In phases with $x > 0$, the extra cations (relative to a M_2O_3 stoichiometry) are accommodated through the formation of Li-rich layers with Li_2MO_3 stoichiometry in the central region of the LN slabs. The proportion of such layers containing extra cations increases in the lower N structures.

ACKNOWLEDGMENTS

The authors thank Colin MacRae for help with the microprobe analyses and Gary Fallon for collecting the CCD intensity data. Support was provided through the National Science foundation, grant DMR 98-09035.

REFERENCES

1. M. E. Villafuerte-Castrejon, A. Aragon-Pina, R. Valenzuela, and A. R. West, *J. Solid State Chem.* **71,** 103–108 (1987).
2. A. Y. Borisevich and P. K. Davies, *J. Am. Ceram. Soc.* **85,** 573–578 (2002).
3. R. I. Smith and A. R. West, *Mater. Res. Bull.* **27,** 277–285 (1992).
4. H. Hayasi, H. Nakano, K. Suzumura, K. Urabe, and A. R. West, *in* "Fourth Euro Ceramics Vol. 2: Basic Science—Developments in Processing of Advanced Ceramics—Part II" (C. Galassi, Ed.), pp. 391–398. Gruppo Editoriale Faenza Editrice, Italy, 1995.
5. R. S. Roth and K. L. Davis, *in* "ACerS Ann. Meet, 89th," p. 88. The American Ceramic Society, Westerville, OH, 1987; also in "Phase Equilibria Diagrams: Volume XI" (R. S. Roth, Ed.), pp. 231–232. The American Ceramic Society, Westerville, OH, 1995.
6. J. C. Mikkelsen, Jr., *J. Am. Ceram. Soc.* **63**(5–6), 331–335 (1980).
7. J. Zou, F. H. Li, D. Y. Yang, Y. D. Jiang, and K. H. Kuo. *Philos. Mag. B* **57**(1), 103–110 (1988).
8. D. Tsubone and T. Shimizu, *J. Cer. Soc. Japan, Intl. Ed.* **101,** 637–641 (1993).
9. P. Bordet, C. Bougerol-Chaillout, I. Grey, J. L. Hodeau, and O. Isnard, *J. Solid State Chem.* **152,** 546–553 (2000).
10. G. M. Sheldrick, "SHELX93, Program for the Refinement of Crystal Structures." University of Gottingen, Germany (1993).
11. S. C. Abrahams, W. C. Hamilton, and J. M. Reddy, *J. Phys. Chem. Solids* **27**(6–7), 1013–1018 (1966).
12. H. Lehnert, H. Boysen, F. Frey, A. Hewatt, and P. Radaelli, *Z. Kristallogr.* **212,** 712 (1997).
13. N. Iyi, K. Kitamura, F. Izumi, J. K. Yamamoto, T. Hayashi, H. Asano, and S. Kimura, *J. Solid State Chem.* **101,** 340 (1992).
14. A. Y. Borisevich and P. K. Davies, *J. Am. Cer. Soc.*, in press.